Egyptian Knowledge Bank
https://ijmti.journals.ekb.eg/

International Journal of
Materials Technology and Innovation
Volume 1, Issue 2 (2021), pages 1-13

Online ISSN 2682-4299

# Promoted photocatalytic hydrogen evolution over core-shell-structured $Co_3O_4/TiO_2$ under visible Light

**M. W. Kadi and R. M. Mohamed***

Department of Chemistry, Faculty of Science, King Abdulaziz University, P.O. Box 80203, Jeddah 21589, Kingdom of Saudi Arabia

*Corresponding author: E-mail: redama123@yahoo.com

Received 27 July 2021
Revised 16 August 2021
Accepted for publication 18 September 2021
Published online 27 September 2021

## Highlights

- Template assisted and sol-gel prepared $Co_3O_4$@$TiO_2$ hollow structures
- Visible light fascination and photocharge separation heightened by adjusting the $Co_3O_4$ nanoshell at 3 wt.%
- Adjusted $Co_3O_4$@$TiO_2$ showed 1820 times higher $H_2$ evolution than pure $TiO_2$
- $Co_3O_4$@$TiO_2$ display excellent recyclability for $H_2$ generation

## Abstract

Our aim in the current work is to focus on a promising and operative method to infuse $Co_3O_4$ into a hollow-structured $TiO_2$ sphere. In this work, we synthesized hollow mesostructured $TiO_2$ nanospheres decorated with $Co_3O_4$ nanoshells through template-based and sol-gel approaches. The produced photocatalysts are p-n heterojunction $Co_3O_4$(shell)@$TiO_2$(core) hollow spheres with a great specific surface area. This mesostructure offers a vast number of photoactive sites for the photocatalytic response. The hexachloroplatinic acid was employed during the photocatalytic action to yield 0.5%Pt/$Co_3O_4$(shell)@$TiO_2$(core) composites. The metallic Pt plays the role of transferring the excited electrons. The nanojunction between the p-$Co_3O_4$ and n-$TiO_2$ can proficiently prohibit the recombination of photocharges. Consequently, resulting in an outstanding photocatalytic hydrogen evolution under visible light. The outstanding photocatalytic activity was due to the hollow structure, the great specific surface area, and the heterostructure between $TiO_2$ and $Co_3O_4$. A practical mechanism for the amended photocatalytic performance was anticipated by enabling the efficiency of charge carrier allocation at $TiO_2/Co_3O_4$ interface. This study offers a perspective toward the design of highly efficient hollow mesostructured photocatalysts for hydrogen production. The technique used to prepare the $TiO_2/Co_3O_4$ nanocomposites is appropriate to fabricate mesoporous mixed oxide photocatalysts for catalysis applications in clean energy production.

## Graphical Abstract

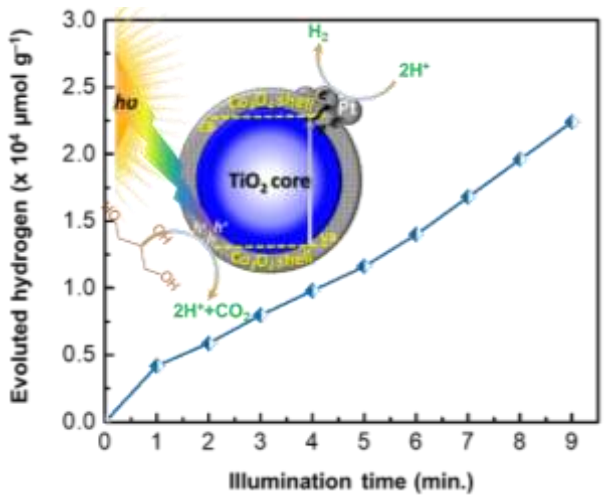


**Keywords:** $Co_3O_4$(shell)@$TiO_2$(core) hollow spheres; Hydrogen production.

 

IJMTI vol. 1, issue 2 (2021) 1- 13 https://doi.org/10.21608/IJMTI.2021.87845.1036

## 1. Introduction

Hole scavenger-assisted hydrogen generation via photocatalysis could be a promising route for clean energy production [1-4]. Numerous researches have been and are still ongoing on $H_2$ generation through water splitting using photocatalysis because of its sustainability and environmental benefits [3–9]. The water-splitting process takes place by the action of a semiconducting photocatalyst, in which the conduction band (CB) edge will have a negative redox potential for $H^+/H_2$ half-reaction (0.0 V vs. NHE) and the valence band (VB) edge will be more positive to the redox potential for $O_2/H_2O$ (1.23 V) half-reaction. $TiO_2$ has been proved to be a good contender for this type of $H_2$ generation process due to its stability, low cost, chemical corrosion resistance, and non-toxic nature compared to various oxides [10–13]. However, yields of $H_2$ over $TiO_2$ are still low for industrial application due to various reasons such as i) the overpotential for $H_2$ evolution on $TiO_2$, ii) rapid recombination of $H_2$ and $O_2$ to form $H_2O$, and iii) the fast recombination of the charge carriers in the reaction vessel [10,14]. To overcome these limitations, alternative approaches can be applied to increase the photocatalytic efficiency of the system. Some approaches include, application of p–n heterojunctions [15-17], doping the semiconductor with a cocatalyst [12,18–20], the addition of sacrificial components, [21], and the application of a Z-scheme combination [22, 23]. For example, metals have been attached to the $TiO_2$ exterior to develop $H_2$ generation yield by reducing recombination processes [10]. The presence of a metal nanoparticle, such as Pt, causes the photo-electrons to occupy a Fermi level ($E_f$) lower in value than that of the CB of $TiO_2$ subsequently enhancing the charge separation [24,25]. In general, noble metals are helpful because of their higher work function and efficient charge separation in enhancing the photoefficiency of the system [11,15,16,26]. Pt is an extremely effective cocatalyst for $H_2$ generation upon doping on $TiO_2$ [27]. Transition metals have also been utilized as cost-effective cocatalysts for visible light response [28, 29]. A major aspect that enhances the photocatalytic ability of the photocatalyst is its specific surface area. High surface area photocatalysts provide adequate responsive spots for photocatalytic progression [30]. The mesoporous hollow-structured spheres represent a morphology that is efficient in light cultivation in the photocatalytic process [31-41].

The $Co_3O_4$-$TiO_2$ p-n heterojunction is typically used in photocatalytic water splitting purposes [42-44]. However, the generated hydrogen from these reported structures was comparatively lower than expected (5000 µmolg$^{-1}$ compared to 22000 µmolg$^{-1}$ in this work) [43], this could be mainly due to the relatively low specific surface area (40~120 m$^2$g$^{-1}$) [44-46]. Hollow-structured core-shell photocatalysts, that are usually synthesized via template-assisted methods exhibit higher surface area [47], lower bandgap [48], and controllable shell/core structure [49]. Additionally, cobalt oxide cocatalysts demonstrate an efficient hydrogen evolution compared to other metal supports [42, 43, 50, 51]. In our method of synthesis, we used Poloxamer 407 as a hydrophilic non-ionic surfactant to obtain a high surface area $SiO_2$ template to guide structuring to increased surface area (400 m$^2$g$^{-1}$) of hollow $TiO_2$ nanosphere for the first time. Thus, the combination of p-n junction $Co_3O_4$@$TiO_2$ hollow sphere structures demonstrate a significant bandgap tuning due to the controllable $Co_3O_4$ shell thickness as well as the high surface area (430 m$^2$g$^{-1}$) that increase the possible number of photoactive sites available for the oxidation-reduction reactions. The solution process offers an easy step for scaling up the preparation of such photocatalysts compared to the complicated routes presently used e.g. atomic layer deposition [45].

## 2. Experimentation

### 2.1. Chemicals

$Ti(OC(CH_3)_3)_4$, cobalt nitrate hexahydrate, Ammonia solution, $C_2H_5OH$, HCl, $CH_3COOH$, hexadecyltrimethylammonium bromide (HTAB), and poloxamer 407 were gained from Sigma-Aldrich.

### 2.2. Preparation of $SiO_2$ hollow nanospheres

The $SiO_2$ hollow nanosphere was formed by the sol-gel technique in the occurrence of poloxamer 407 and hexadecyltrimethylammonium bromide (HTAB) as surfactants according to the following steps: 20 mL of deionized water, 40 mL ethanol, 1.5 g hexadecyltrimethylammonium bromide, 4.5 g of poloxamer 407, 2.35 mL of acetic acid and 0.75 mL of HCl were mixed and the resulting mixture was stirred at 27°C for 60 min. The 0.4 mL of TEOS was then added to the solution and the obtained combination was stirred for 60 min. Ethanol was evaporated at 40 °C for 24 h and the $SiO_2$ hollow nanospheres were gained.

### 2.3. Preparation of Hollow mesoporous $TiO_2$ nanosphere

0.5 g of the formed $SiO_2$ nanospheres was dissolved in 40 mL of ethyl alcohol. Then, a mixture of 0.4 mL ammonium hydroxide solution and 0.4 mL hexadecyltrimethylammonium bromide was added to

IJMTI vol. 1, issue 2 (2021) 1- 13 https://doi.org/10.21608/IJMTI.2021.87845.1036

the above suspension with stirring for 15 min. After that, 0.4 mL of titanium sec-butoxide was then introduced and the stirring was kept for another 30 min in ambiance. To produce the hollow mesoporous $TiO_2$ nanospheres, the $SiO_2$@$TiO_2$ sample was dehydrated in the air at 40 ○C for 24 h and then calcinated for 4 h at 500 ○C using a 1°C/min heating rate. Hollow mesoporous $TiO_2$ nanospheres were collected by etching $SiO_2$ core in NaOH aqueous solution at 90 °C.

### 2.4. Preparation of $Co_3O_4$(shell)@$TiO_2$(core) hollow mesoporous nanospheres

Hollow mesoporous nanosphere $Co_3O_4$@$TiO_2$ nanocomposites were prepared as in the following steps: 0.5 g of hollow mesoporous $TiO_2$ nanosphere was dispersed in 40 mL deionized water and 10 mL of acetic acid. Then, 0.01 g of cobalt nitrate was added and the obtained mixture was left at room temperature for 60 min. The hollow mesoporous nanospheres $Co_3O_4$@$TiO_2$ were finally produced by dehydrating the mixture at 40 °C for 24 h and then calcination in the air for 4 h at 400 °C using 1°C/ min heating rate. This method with repeated three times to prepare different weight percent of x% $Co_3O_4$ to $TiO_2$ where x=0, 1, 2, 3, and 4 wt.%.

### 2.5. Characterization

The structure morphology for hollow nanospheres of $TiO_2$ and $TiO_2$/$Co_3O_4$ nanocomposites was investigated using a JEOL-JEM-1230 transmission electron microscope (TEM) and a JEOL-JSM-5410 scanning electron microscope (SEM). The crystalline structure of x%$Co_3O_4$@$TiO_2$ nanocomposites was obtained by Bruker axis D8 X-ray diffractometer utilizing Cu Kα radiation (λ=1.540 Å). The $N_2$ adsorption/desorption isotherms were observed at 77 K by a Chromatech apparatus (Nova 2000 series) after degassing at 150 °C. The elemental analysis was investigated through the core-level X-ray photoelectron spectra (XPS) measurements via K-ALPHA spectrometer (Thermo Scientific). The diffusive reflectance (DRS) of the obtained materials was chronicled at room temperature by JASCO a V-570 spectrophotometer. The $E_g$ was calculated from the DRS by the Tauc formula. The photocharge recombination studies were investigated through photoluminescence (PL) spectra of gained structures via RF-5301 fluorescence spectrophotometer (Shimadzu). The vibrational spectra of the obtained samples were studied via a Perkin-Elmer spectrophotometer at a resolve of 4.0 wavenumber FTIR spectrometer in the range 4000-400 $cm^{-1}$. Raman depiction was done by Horiba Lab RAM instrument applying 523.5 nm from Ar ion laser. Finally, Zahner Zennium electrochemical workstation was cast to measure the photocurrent intensity and to measure transient photocurrent.

### 2.6. Photocatalytic $H_2$ generation

The photoactivity of the $Co_3O_4$(shell)@$TiO_2$ (core) nanospheres for $H_2$ generation was examined in a 250 mL photocell having a water circulator system. A 500 W Xe light source with a cutoff filter (<420 nm) was immobile in a horizontal manner on the photocell. a pre-calculated dose of the obtained photocatalyst was dispersed in 10 vol% of glucose solutions. the metallic Pt was photodeposited on the $Co_3O_4$@$TiO_2$ nanospheres by photoreduction during the photoreaction of $H_2$ generation. Typically, 26 µL of 50 mM of hexachloroplatinic acid was added to the photocell. Before the photoreaction, Ar gas was bubbled for 15 min to eradicate oxygen. The illumination period for the photoreaction was 9 hours. The $H_2$ progression was followed by the Agilent GC 7890A gas chromatograph.

## 3. Results and Discussion

### 3.1. Materials Preparation and Characterization

The XRD diffractograms of the obtained samples with various contents of $Co_3O_4$ are described in Fig. 1. The produced $TiO_2$ and x%$Co_3O_4$@$TiO_2$ nanocomposites were mainly of the anatase phase. The characteristic diffraction positions at (2$\theta$) =25.2°, 37.8°, 48.0°, 53.7°, 54.9°, and 62.2° are in typical coincidence with the (*hkl*) index planes represented in Fig. 1 [52].

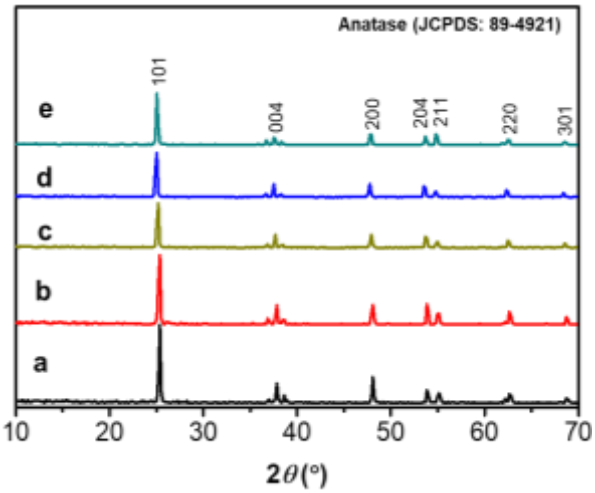


**Fig. 1** X-ray diffraction patterns of samples at different wt% of $Co_3O_4$ source at 0, 1,2,3, and 4 as represented by a, b, c, d, and e, individually.

IJMTI vol. 1, issue 2 (2021) 1- 13 https://doi.org/10.21608/IJMTI.2021.87845.1036

It should be noticed that the main (101) intensity was reduced by incorporating the 1~4 wt.% of the Co source. There was no indication of any other impurity phases in all samples.Fig. 2 shows the $N_2$ adsorption/desorption isotherms of the hollow-structured $TiO_2$ with 1 and 3 wt.% $Co_3O_4$ as indicated. The isotherms unveiled the characteristic H3 hysteresis type IV loop, [53]. This feature suggests a mesoporous structured composite [54, 55].

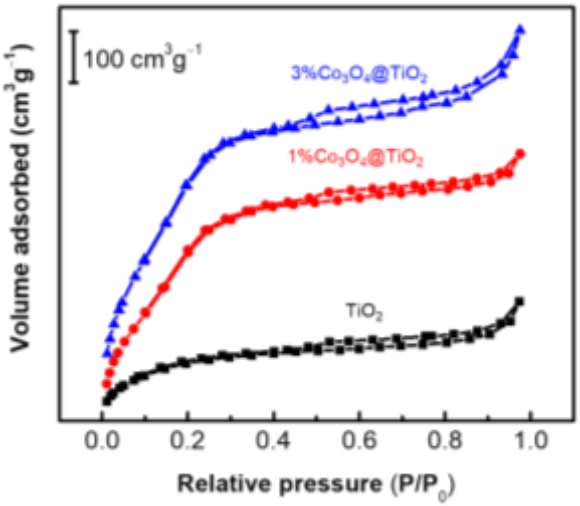


**Fig. 2** Nitrogen adsorption/desorption isotherms of selected hollow-structured $TiO_2$ (black) compared to 1.0 and 3.0 wt.% $Co_3O_4$@$TiO_2$ nanocomposites (red and blue).

The specific surface texture in terms of surface area and volumetric measure of pure $TiO_2$ are 401 $m^2$ $g^{-1}$ and 0.490 $m^3$ $g^{-1}$, correspondingly. the surface texture parameters are progressively augmented by the addition of $Co_3O_4$-coated the hollow nanosphere (Table 1). The 4 wt.% $Co_3O_4$/$TiO_2$ nanocomposite displayed a 430 $m^2 g^{-1}$ of surface area and 0.580 $m^3 g^{-1}$ for the pore volume [52, 56]. The surface characteristics of all the synthesized nanocomposites with varying $Co_3O_4$ are presented abridged in Table 1. The characteristic structural surface of the $Co_3O_4$@$TiO_2$ nanocomposites is predicted to indorse the $H_2$ evolution.

The morphological structures of the produced samples are depicted through the SEM and TEM images as presented in Fig. 3 and Fig. 4, correspondingly. The $SiO_2$ template is seen in Fig. 3A with a diameter of about 120 nm showing a flat spherical exterior. While the produced $TiO_2$ spheres are also extant a flat superficial with little increase of size (130 nm) as seen in both Figs. 3b and 4A. The hollow-mesoporous $TiO_2$ spheres with a bumpy shallow seen with a similar diameter pure $TiO_2$ (Fig. 3C, Fig. 4B) upon loading with 1% of Co. The presence of rough nanoparticles is referred to as the small loading of the $Co_3O_4$. As presented the $Co_3O_4$ nano-shell with ~20 nm is composed of small nanoparticles.

Figs. 3D~F and Figs.4 C~F are showing that the surface of the hollow-structured $TiO_2$ spheres having a rough decoration of $Co_3O_4$ nanoshells.

Fig. 4E displays the lattice parameter of the shell and the core at 0.25 and 0.34 nm, which is credited to the (311) plane of $Co_3O_4$ and the (101) plane of anatase $TiO_2$ [29,57]. The thin-layered structure of $Co_3O_4$ is composed of small flake-like particles covering the $TiO_2$ hollow spheres. This designated structure can offer super active sites for photocharge conduction upon light illumination. Furthermore, the $Co_3O_4$ (shell)@$TiO_2$(core) exhibits a close heterojunction interface indicating an improved subsequent photoactivity.

The elemental and chemical composition of the prepared photocatalyst was revealed through XPS analysis of the selected 3%$Co_3O_4$@$TiO_2$ sample as displayed in Fig. 5. The Ti 2p band exposed in Fig. 5a discloses two core peaks at 458.2 and 464.1 eV for the chemical states of $Ti^{3+}$ and $Ti^{4+}$ [57]. The Co 2p XPS core level (Fig 45B) shows two doublets at 796.5 eV ($2p_{1/2}$) -780.2eV ($2p_{3/2}$) and 789.0 eV($2p_{1/2}$)-803.6 eV($2p_{3/2}$) assigned to $Co^{3+}$ and $Co^{2+}$ states, individually. The cohabitation of the $Co^{2+}$ and $Co^{3+}$ species is also confirmed from the spin-orbit splitting of 14.6 eV and the satellite peaks around 790 and 805 eV [58]. The co-occurrence of $Co^{3+}$ and $Co^{2+}$ agrees with the existence of $Co_3O_4$ on the exterior of the $TiO_2$/$Co_3O_4$-3wt% nanocomposites. As well, the O 1s band in Figure 5C shows one peak at 531.4 eV, which is deconvoluted to the oxide-structured $TiO_2$ or $Co_3O_4$ (531.4 eV), and the $^-$OH assemblies adsorbed onto the sample's surface (532.6 eV) [57,58].

Supplementary investigation for the structure of the x%$Co_3O_4$@$TiO_2$ was attained by Raman spectroscopy as in Fig. 6A. The Raman spectra present discrete bands situated at 145, 420, and 516 $cm^{-1}$, which signify the vibrant Eg, B1g, and A1g modes of the anatase phase [59]. The addition of the $Co_3O_4$ shell into the $TiO_2$ did not alter the Raman spectra except for the intensity of the vibrational modes. The Raman bands of $Co_3O_4$ lies in the same range of the anatase one as 146 $cm^{-1}$ ascribed to Co lattice vibrations are overlain with the $TiO_2$. The observed Raman bands for the $Co_3O_4$ at 147, 387, and 515 $cm^{-1}$ for tetrahedral F2g symmetry of $CoO_4$ according to the literature [60]. The functional groups within x% $Co_3O_4$@$TiO_2$ hollow spheres were analyzed via FT-IR spectroscopy as in Fig 6B. The spectra display discrete bands at 3565, 3385, 2340, 1627, 1498, 1341, 775, and 610 $cm^{-1}$ which are all

IJMTI vol. 1, issue 2 (2021) 1- 13 https://doi.org/10.21608/IJMTI.2021.87845.1036

indicating the typical spectra of functionalized $TiO_2$ [51]. The band located at 1627 $cm^{-1}$ the broader centered at 3385 $cm^{-1}$ are linked to chemisorbed or physisorbed water molecules [61]. Also, the wideband located at 3565 $cm^{-1}$ could be ascribed to the –OH group. While the 2340 $cm^{-1}$ vibration belongs to the physical attachment of $CO_2$. The lower intensity features around 1341 and 1498 $cm^{-1}$ may be ascribed to superficial carbonate type designed by the presence of $Co_3O_4$@$TiO_2$ in ambiance [60,62,63]. Lastly, the extensive band at 610~775 $cm^{-1}$ is situated within the Ti-O-H bending mode [63].

**Table 1** Effect of $Co_3O_4$ nanoshell addition on the physicochemical characteristics of synthesized $TiO_2$ hallow spheres.

| Sample | $S_{BET}$ ($m^2$/g) | Pore volume ($cm^{-3}$ $g^{-1}$) | Abs. edge (nm) | $E_g$ (eV) | PL peaks (nm) | Generated $H_2$ (μmol $g^{-1}$) |
|---|---|---|---|---|---|---|
| $TiO_2$ | 400.0 | 0.488 | 392 | 3.43 | 388 | 10 |
| 1%$Co_3O_4$@$TiO_2$ | 410.0 | 0.520 | 409 | 3.05 | 416 | 4200 |
| 2%$Co_3O_4$@$TiO_2$ | 420.0 | 0.540 | 447 | 2.94 | 478 | 14000 |
| 3%$Co_3O_4$@$TiO_2$ | 425.0 | 0.570 | 506 | 2.6 | 557 | 18200 |
| 4%$Co_3O_4$@$TiO_2$ | 430.0 | 0.580 | 507 | 2.57 | 557 | 18240 |

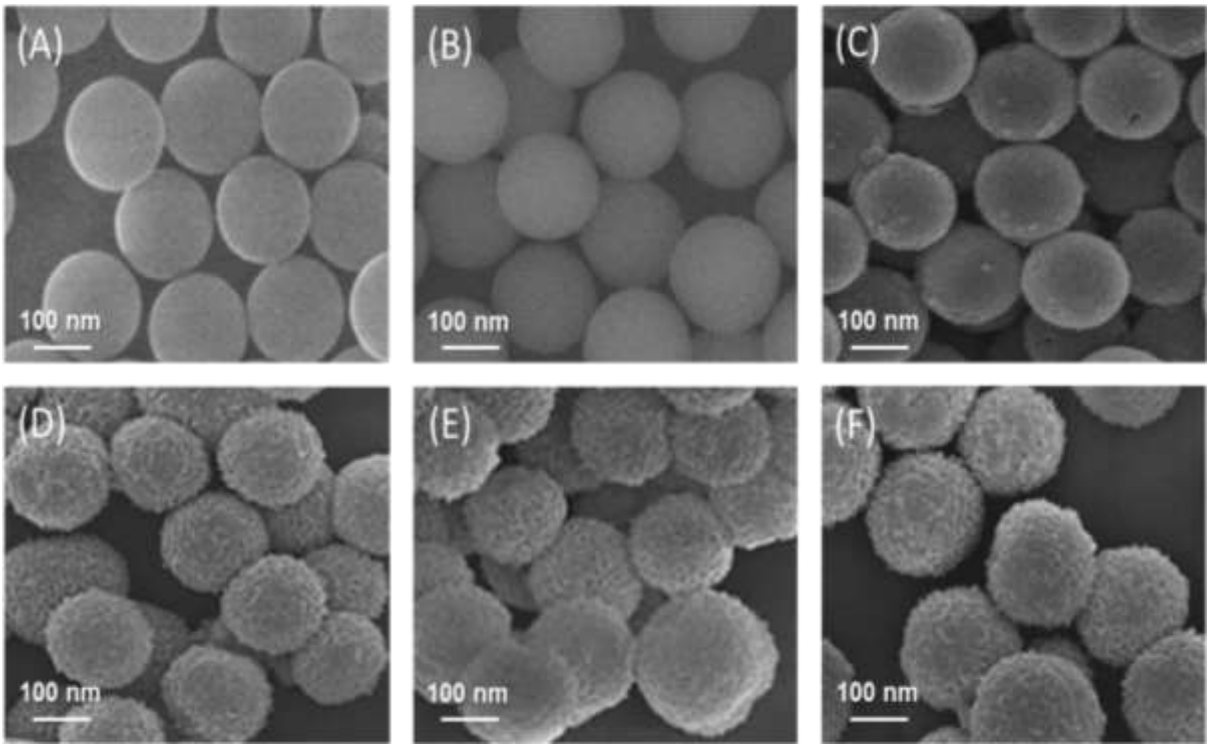


**Fig. 3** SEM images of pure $SiO_2$ hollow spheres (A) and x% $Co_3O_4$@$TiO_2$ nanocomposites at x=0.0 (B), 1.0 (C), 2.0 (D), 3.0 (E), and 4.0 (F).

IJMTI vol. 1, issue 2 (2021) 1- 13 https://doi.org/10.21608/IJMTI.2021.87845.1036

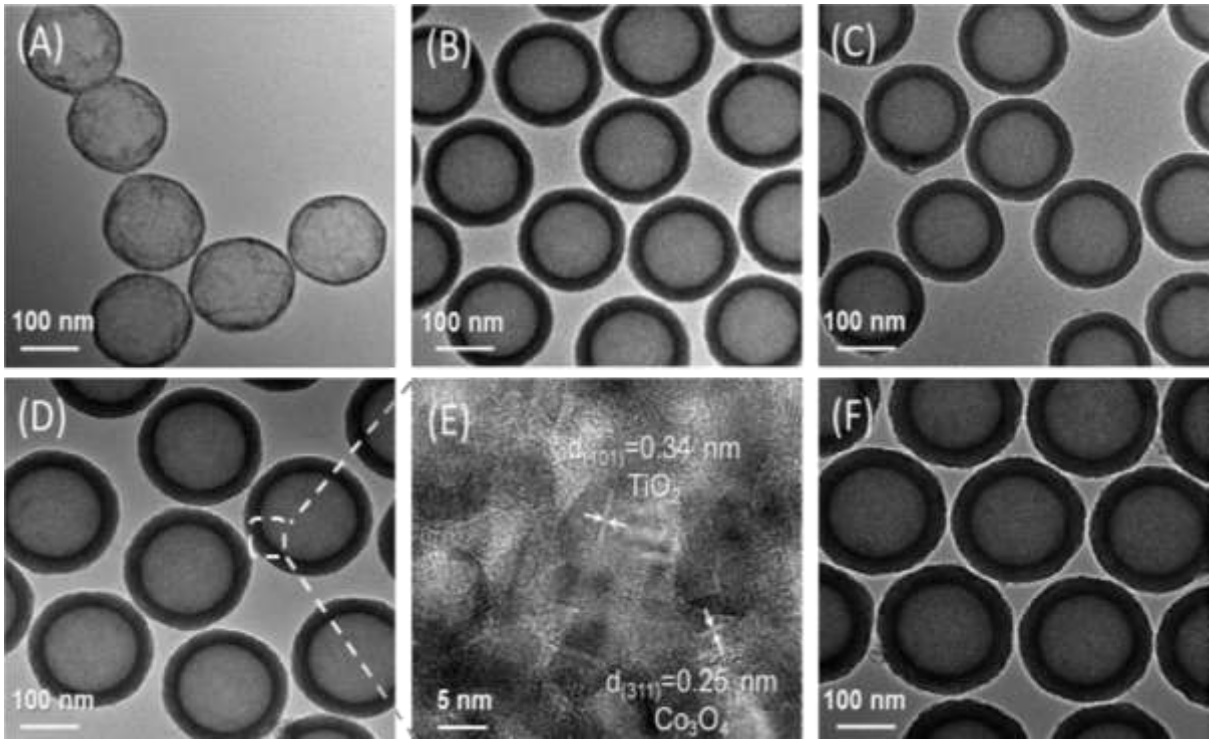


**Fig. 4** TEM images of pure $TiO_2$ hollow spheres (A) and x% $Co_3O_4$(shell)@$TiO_2$(core) nanocomposites at x=1.0(B), 2.0 (C), 3.0 (D) and 4.0 (F). The high-resolution TEM image of (D) showing lattice parameters for $Co_3O_4$ and $TiO_2$ represented in (E).

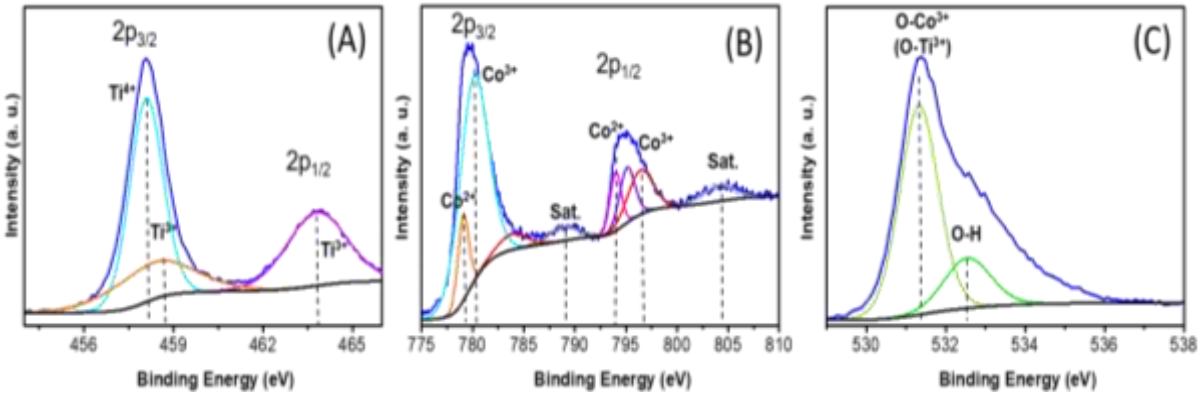


**Fig. 5** High-resolution XPS of 3.0$Co_3O_4$@$TiO_2$ nanocomposite showing Ti2p (A), Co2p (B), and O1S in (C).

Fig. 7A displays the UV-vis DRS of the x%$Co_3O_4$@$TiO_2$ nanocomposites compared to the bare mesoporous $TiO_2$ hollow spheres. The bare $TiO_2$ exhibited a sizable enhancement of efficiency in light-harvesting by the introduction of $Co_3O_4$ nanoshells. The optical density in the visible range is enhanced as well. Thus, the close contact between the p-type $Co_3O_4$ and n-type $TiO_2$ amended the interfacial band edges resulting in the acceleration of photocharge production [64]. The estimated $E_g$ of mesoporous $TiO_2$ is 3.43 eV, in contrast, the $Co_3O_4$@$TiO_2$ provides a wider light absorption capability due to its narrower $E_g$ of ~2.57 eV (Table 1, Fig. 7B). The reduction of $E_g$ and the upsurge of the visible-light absorption for the $Co_3O_4$@$TiO_2$ nanocomposites might be clarified by the impacts of nanoscale surface plasmon resonance [65,66] or the charge allocation in optical transitions between the $TiO_2$ core and the $Co_3O_4$ shell.

IJMTI vol. 1, issue 2 (2021) 1- 13 https://doi.org/10.21608/IJMTI.2021.87845.1036

### 3.2. Photocatalytic $H_2$ evolution

The p–n heterojunction is fabricated by the amalgamation of p-type $Co_3O_4$ nanoshell and n-type $TiO_2$ core fashions in an electric field with band orientation. These core-shell nanocomposite hollow spheres powerfully ease the parting of photocharges and surging the photoefficiency [34,63,64]. The photocatalytic action of hollow-structured $TiO_2$ spheres and x%$Co_3O_4$@$TiO_2$ nanocomposites was utilized for $H_2$ generation under the illumination of visible light using glucose (10 vol% in $H_2O$) as a hole scavenger. The photosystem contains the $H_2PtCl_6$ deposits Pt nanoparticles on the surface of $Co_3O_4$@$TiO_2$. As seen in Fig. 8A, if $TiO_2$ was only used as a sole photocatalyst, trivial $H_2$ generation was observed (~10 µmol/g, Table 1). The poor photocatalytic $H_2$ generation utilizing the only $TiO_2$ is due to the accelerated photocharge recombination and the large overpotential for $H_2$ generation. The x%$Co_3O_4$@$TiO_2$ heterojunction showed enhanced photoefficiency toward hydrogen evolution (Fig. 8a, Table 1). The mesoporous $Co_3O_4$@$TiO_2$ nanocomposites produced cumulative amounts of $H_2$ in an exponential trend through the photocatalytic reaction due to the higher photoactivity under visible light.

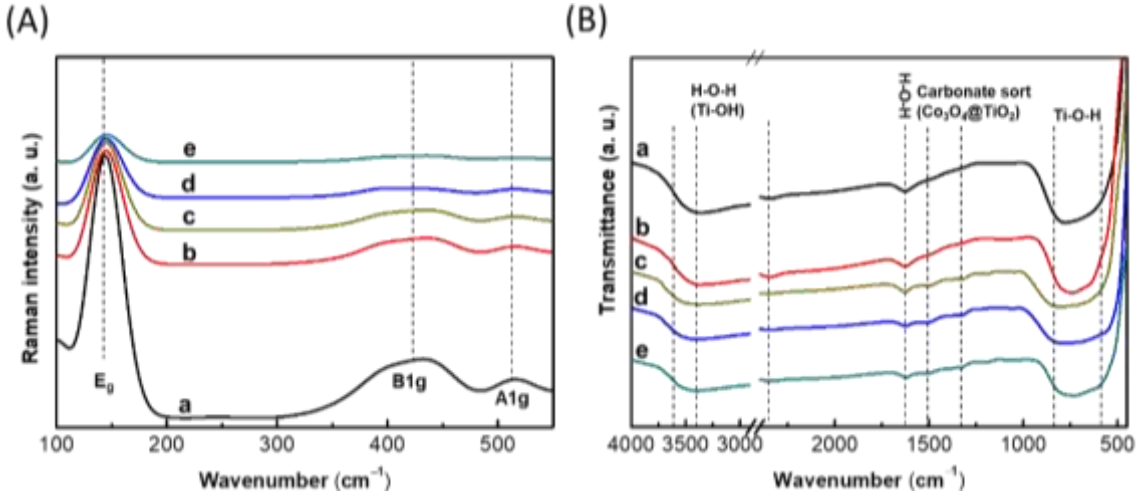


**Fig. 6** Raman (A) and (B) FTIR spectra investigation of samples of various wt.% of Co source at 0, 1,2,3, and 4 % as signified by a, b, c, d, and e, correspondingly.

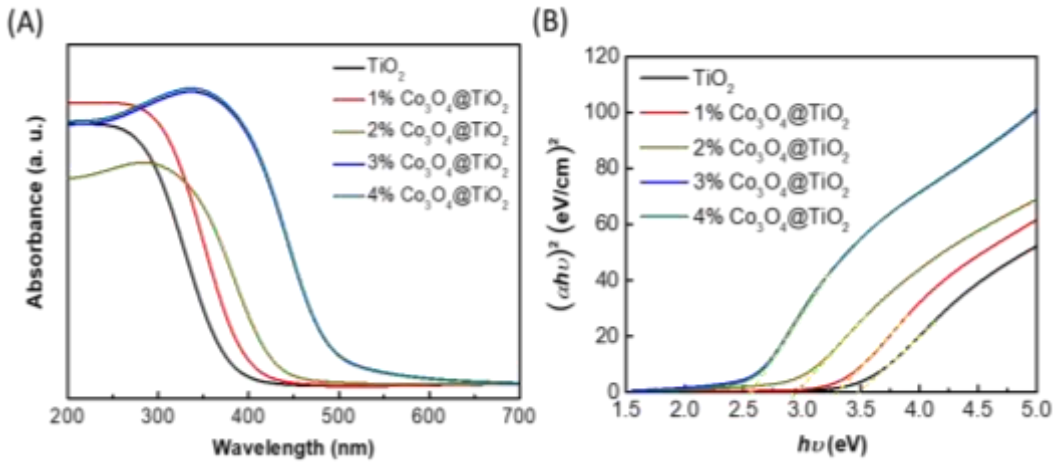


**Fig. 7** UV-vis DRS of hollow-structured $TiO_2$ spheres compared to $Co_3O_4$@$TiO_2$ nanocomposites as designated in (A). The assessed bandgap using the Tauc plot in (B).

IJMTI vol. 1, issue 2 (2021) 1- 13 https://doi.org/10.21608/IJMTI.2021.87845.1036

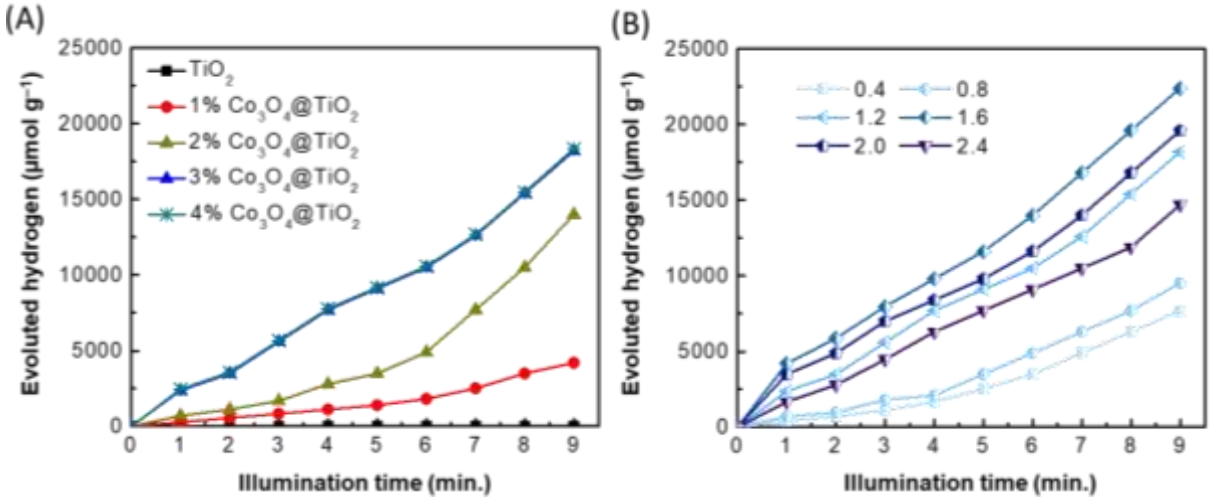


**Fig. 8** Photocatalytic hydrogen progress against illumination time by applying diverse $Co_3O_4$-loaded $TiO_2$ core-shell structures as indicated in (A). The impact of the photocatalyst amount of the best 3%$Co_3O_4$@$TiO_2$ photocatalyst is presented in (B).

The $H_2$ generation reached 18200 µmol/g after 9 h of light radiation by adding the $Co_3O_4$ nanoshell up to 3 wt%. The total $H_2$ was 1820 times superior to the bare $TiO_2$. The presence of $Co_3O_4$ leads to the creation of suitable valance and conduction band positions for $H_2$ formation reaction. Fig. 8B illustrates the impact of 3%$Co_3O_4$@$TiO_2$ concentration from 0.4~2.4 g/L on the photogeneration of $H_2$ within the 9h irradiation period. At the lowest dose of 0.4 g/L of 3%$Co_3O_4$@$TiO_2$ nanocomposite, the photogenerated $H_2$ evolution was ~ 7700 µmol/g. By increasing the dose to 1.6 g/L, the photogenerated $H_2$ enhanced to 22400 µmol/g compared to 9250 and 18200 µmol/g for 0.8 and 1.2 g/L, singly. The further increase of the optimized photocatalyst to 2.4 g/L reduced the amount of generated $H_2$ to 14700 µmol/g. Thus, the optimal dose of the 3%$Co_3O_4$@$TiO_2$ nanocomposite was fixed at 1.6 g/L. The possible reasons for dropping the $H_2$ photogeneration could be the lessening of photoactive sites or the inefficient photon scattering due to the opacity of 3%$Co_3O_4$@$TiO_2$ that inhibits light photons [3,15,26]. The existence of the mesostructured hollow 3%$Co_3O_4$@$TiO_2$ heterojunctions enhances light collecting and reflection, the diffusion of glucose molecules scavenges the holes, and the high surface area of the material result in the observed superior photocatalytic efficiency. The reusability of the spent Pt/3%$Co_3O_4$@$TiO_2$ photocatalyst was investigated in Fig. 9. The generation of $H_2$ evolution over the reused photocatalyst was slightly decreased keeping ~98% of the original $H_2$ amount after the fifth cycle.

To understand why the 3%$Co_3O_4$@$TiO_2$ is the optimal photocatalyst, we investigated the PL spectra of x%$Co_3O_4$@$TiO_2$ compared to the pure $TiO_2$ hollow spheres as in Fig. 10A. The pure $TiO_2$ displayed a PL feature around 388 nm with relatively higher power than other samples. Nevertheless, the PL features of x%$Co_3O_4$@$TiO_2$ nanocomposites unveiled a redshift to the wavelength of 557 nm for the 3%$Co_3O_4$@$TiO_2$ with the lowest intensity (table 1). The reduction in the PL signal in this sample specifies the movement of electrons from the CB of $TiO_2$ to the CB of $Co_3O_4$ [66].

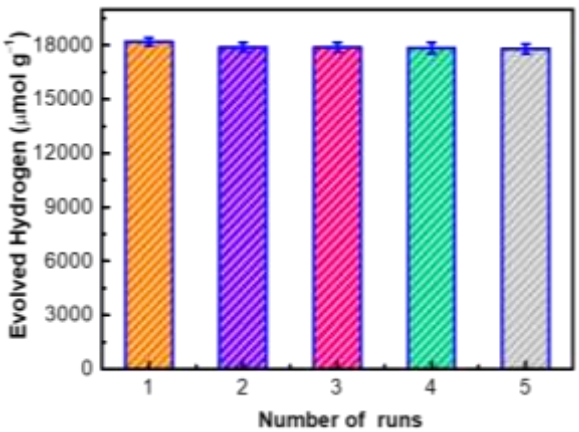


**Fig. 9** The constancy of the improved dose of 3%$Co_3O_4$@$TiO_2$ hollow core-shell-structured photocatalyst with maintainable hydrogen production level after five consecutive cycles.

The subordinate emission of the 3%$Co_3O_4$@$TiO_2$ is due to the recombination suppression of the photocharges upon irradiation. Afterward, the electrons easily move to bend the Fermi level to less value. This results in a higher reductive ability of 3%$Co_3O_4$@$TiO_2$.

IJMTI vol. 1, issue 2 (2021) 1- 13 https://doi.org/10.21608/IJMTI.2021.87845.1036

Concurrently, the modified trapped states imply an efficient electron-hole separation that subsequently enhances the evolution of $H_2$ [57, 66]. These outcomes were further confirmed by measuring the photocurrent intensity during light irradiation, as shown in Fig. 10B. According to the photocurrent results, the photocurrents for x%$Co_3O_4$@$TiO_2$ were increased by increasing the $Co_3O_4$ nanoshells compared to a negligible photoresponse by only $TiO_2$. The intense photocurrent indicates that 3%$Co_3O_4$@$TiO_2$ possess the highest ability to transfer the photogenerated carriers upon illumination [67].

The proposed mechanism regarding the photocatalytic generation of $H_2$ utilizing Pt/ 3%$Co_3O_4$@$TiO_2$ is presented in Fig. 11. The $Co_3O_4$-coated $TiO_2$ hollow sphere's surface works to reduce the recombination of the charge carriers by advancing the holes from $TiO_2$ to $Co_3O_4$ and electrons to the photo-deposited Pt. The holes at the $Co_3O_4$ are captured by the glucose scavenger to produce protons. The electrons on the Pt surface can then oxidize the protons to produce $H_2$ on Pt particles [11,26,66]. The substantial narrowing of the $E_g$ of the 3%$Co_3O_4$@$TiO_2$ heterostructures was a reason for the favorable response to light illumination. Furthermore, the modified energy levels due to the close connection of the core-shell structure functionalize the hole-trapping spots that balance the potential of the $H^+/H_2$ reaction. This eventually moves the electrons to the Pt nanoparticle which meets the glucose dispersed through the pores of the $Co_3O_4$@$TiO_2$ heterojunction. the glucose itself, like a scavenging agent, eats the holes. Thus, the placid electrons by Pt are transported to $H^+$ to form $H_2$ (Fig. 11).

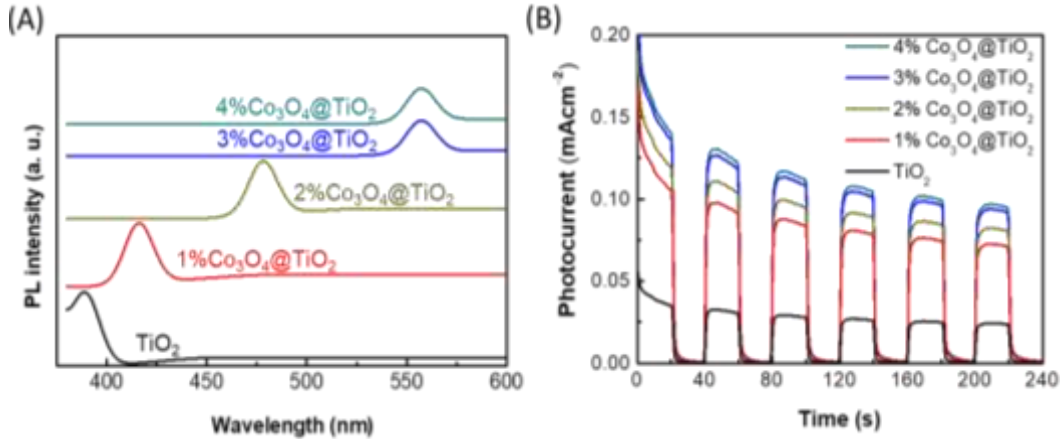


**Fig. 10** PL spectra (A) and transient photocurrent intensity (B) of pure $TiO_2$ hollow spheres compared to x%$Co_3O_4$@$TiO_2$.

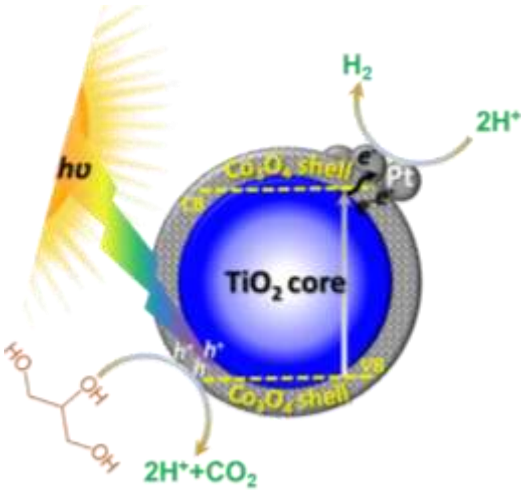


**Fig. 11** Photocatalytic hydrogen production scheme by the 3%$Co_3O_4$@$TiO_2$ nanocomposite.

The photoproduction of $H_2$ in this way is being considerably augmented due to the synergy between the Pt and the constructed $Co_3O_4$(shells)@$TiO_2$(cores) photocatalyst.

## 4. Conclusion

We have effectively synthesized a novel hollow-structured $Co_3O_4$(shell)/$TiO_2$(core) photocatalysts by template-based and sol-gel approaches with templates used for the first time. The 3% $Co_3O_4$-coated $TiO_2$ sample demonstrated the highest photoactivity for hydrogen generation under visible light illumination compared to the parent bare $TiO_2$ hollow spheres. The $H_2$ production rate was measured to be 10 μmol $h^{-1}$ $g^{-1}$ over the pure hollow $TiO_2$, and it was as high as 1820 times more when 3% $Co_3O_4$-coated $TiO_2$

nanocomposite was used. The optimal $Co_3O_4$ shell content decorated on $TiO_2$ was 3%. The $H_2$ generation was significantly enhanced by the synergetic impacts between Pt and $Co_3O_4$ on $TiO_2$ hollow spheres. The presence of hollow-structured $Co_3O_4$(shell)/$TiO_2$(core) photocatalysts potentially enhanced light-harvesting making the synthesized hollow-structured $Co_3O_4$(shell)/$TiO_2$(core) more active harvesters of photons. The increased dissemination of glucose molecules due to the advanced surface area resulted also in augmented efficiency of a superior number of photoactive sites. The brilliant photocatalytic presentation was due to the hollow structure, the sufficient specific surface area, and the heterostructure between $TiO_2$ and $Co_3O_4$. A sensible mechanism for the amended photocatalytic efficacy was anticipated by enabling the efficiency of charge carrier allocation at $TiO_2$/$Co_3O_4$ interface. This study offers a perspective toward the design of highly effective hollow mesoporous photocatalysts for hydrogen production. The technique used to create the $TiO_2$/$Co_3O_4$ nanocomposites is adequate to fabricate mesoporous mixed oxide photocatalysts for catalysis applications in clean energy production.

## Acknowledgements

This Project was funded by the Deanship of Scientific Research (DSR) at King Abdulaziz University, Jeddah, under grant no. **P-93.** The authors, therefore, acknowledge with thanks DSR for technical and financial support.

## References

[1] A. Fujishima and K. Honda, Electrochemical photolysis of water at a semiconductor electrode, Nature, 238 (1972)37–38.

[2] K. Maeda and K. Domen, Photocatalytic water splitting: recent progress and future challenges, J. Phys. Chem. Lett., 1(2010) 2655–2661.

[3] M. W. Kadi, R. M. Mohamed, A. A Ismail, D. W. Bahnemann, Decoration of mesoporous graphite-like $C_3N_4$ nanosheets by NiS nanoparticles driven visible light for hydrogen evolution, Applied Nanoscience, 8 (2018)1587-1596.

[4] A. A. Ismail and D. W. Bahnemann, Photochemical splitting of water for hydrogen production by molecular photocatalysis: A Review, Solar Energy Materials & Solar Cells, 128 (2014)85-101.

[5] H. Tang, C. M. Hessel, J. Wang, N. Yang, R. Yu, H. Zhao andD. Wang, Two-dimensional carbon leading to new photoconversion processes, Chem. Soc. Rev., 43(2014)4281–4299.

[6] J. Qi, K. Zhao, G. Li, Y. Gao, H. Zhao, R. Yu and Z. Tang, Multi-shelled $CeO_2$ hollow microspheres as superior photocatalysts for water oxidation, Nanoscale, 6 (2014) 4072–4077.

[7] S. Wang, L. Yi, J. E. Halpert, X. Lai, Y. Liu, H. Cao, R. Yu, D. Wang, and Y. Li, A novel and highly efficient photocatalyst based on P25–graphdiyne nanocomposite, Small, 8 (2012) 265–271.

[8] N. Yang, Y. Liu, H. Wen, Z. Tang, H. Zhao, Y. Li and D. Wang, Photocatalytic Properties of Graphdiyne and Graphene Modified $TiO_2$: From Theory to Experiment, ACS Nano, 7 (2013)1504–1512.

[9] D. Barreca, G. Carraro, V. Gombac, A. Gasparotto,C. Maccato, P. Fornasiero and E. Tondello, Supported metal oxide nanosystems for hydrogen photogeneration: Quo vadis? Adv. Funct. Mater., 21(2011)2611–2623.

[10] R. M. Mohamed, Characterization and catalytic properties of nano-sized Pt metal catalyst on $TiO_2$-$SiO_2$ synthesized by photo-assisted deposition and impregnation methods. Journal of materials processing technology, 209 (2009) 577-583.

[11] T. A. Kandiel, A. A. Ismail, D. W. Bahnemann, Mesoporous $TiO_2$ nanostructures: a route to minimize Pt loading on titania photocatalysts for hydrogen production, Physical Chemistry Chemical Physic, 12(2011)20155-20161.

[12] R. M. Mohamed, and E. Aazam, Synthesis and characterization of P-doped $TiO_2$ thin-films for photocatalytic degradation of butyl benzyl phthalate under visible-light irradiation. Chinese Journal of Catalysis, 34(2013)1267-1273.

[13] A. A. Ismail, T. A. Kandiel, D. W. Bahnemann, Novel (and better?) titania-based photocatalysts: brookite nanorods and mesoporous structures, J. Photochem. Photobiol., A, 216 (2010)183-193.

[14] Z. Jin, X. Zhang, Y. Li, S. Li and G. Lu, 5.1% Apparent quantum efficiency for stable hydrogen generation over eosin-sensitized CuO/$TiO_2$ photocatalyst under visible light irradiation, Catal. Commun., 8 (2007)1267–1273.

[15] H. Alshaikh, A. Shawky, R.M. Mohamed, J. G. Knight, L. S. Roselin, Solution-based synthesis of $Co_3O_4$/ZnO p-n heterojunctions for rapid visible-light-driven oxidation of ciprofloxacin, Journal of

Molecular Liquids 334 (2021) 116092. R. M. Mohamed, M.A., Salam, Photocatalytic reduction of aqueous mercury (II) using multi-walled carbon nanotubes/Pd-ZnO nanocomposite, Materials Research Bulletin 50 (2014) 85-90.

[16] M. H. Lee, K. Takei, J. Zhang, R. Kapadia, M. Zheng,Y.-Z. Chen, J. Nah, T. S. Matthews, Y.-L. Chueh, J. W. Ager and A. Javey, p-Type InP nanopillar photocathodes for efficient solar-driven hydrogen production, Angew. Chem., Int. Ed., 51 (2012)10760–10764.

[17] R. M. Mohamed, I.A. Mkhalid, E.S. Baeissa, M.A.Al-Rayyani, Photocatalytic degradation of methylene blue by Fe/ZnO/$SiO_2$ nanoparticles under visible light. Journal of Nanotechnology 2012 (2012) 329082.

[18] R. M. Mohamed, I. A. Mkhalid, A. Shawky, A Facile synthesis of Pt–In2O3/BiVO4 nanospheres with improved visible-light photocatalytic activity. J Alloys Compd 775(2019)542–548.

[19] J. Yu and J. Ran, Facile preparation and enhanced photocatalytic $H_2$-production activity of $Cu(OH)_2$ cluster modified $TiO_2$, Energy Environ. Sci., 4(2011)1364–1371.

[20] A. Shawky, R. M. Mohamed, I. A. Mkhalid, N. S. Awwad, H. A. Ibrahium, One-pot synthesis of $Mn_3O_4$-coupled $Ag_2WO_4$ nanocomposite photocatalyst for enhanced photooxidative desulfurization of thiophene under visible light irradiation, Applied Nanoscience, 8 (2018) 1179-1188.

[21] H. Tada, T. Mitsui, T. Kiyonaga, T. Akita and K. Tanaka, All-solid-state Z-scheme in CdS–Au–$TiO_2$ three-component nanojunction system, Nat. Mater., 5 (2006)782–786.

[22] H. J. Yun, H. Lee, N. D. Kim, D. M. Lee, S. Yu and J. Yi, A combination of two visible-light responsive photocatalysts for achieving the Z-scheme in the solid state, ACS Nano, 5(2011) 4084 –4090.

[23] M. Jakob, H. Levanon and P. V. Kamat, Charge distribution between UV-irradiated $TiO_2$ and gold nanoparticles: Determination of shift in the fermi level, Nano Lett., 2003, 3, 353–358.

[24] V. Subramanian, E. E. Wolf, P. V. Kamat, Catalysis with $TiO_2$/gold nanocomposites. Effect of metal particle size on the fermi level equilibration, J. Am. Chem.Soc., 126 (2004) 4943–4950.

[25] A. Shawky, M. Alhaddad, K.S. Al-Namshah, R. M. Mohamed, N.S. Awwad, Synthesis of Pt-decorated CaTiO3 nanocrystals for efficient photoconversion of nitrobenzene to aniline under visible light, J. Mol. Liq. 304 (2020) 112704.

[26] G. L. Chiarello, M. H. Aguirre and E. Selli, Hydrogen production by photocatalytic steam reforming of methanol on noble metal-modified $TiO_2$**,** J. Catal., 273 (2010)182–190.

[27] V. Artero, M. Chavarot-Kerlidou and M. Fontecave, Splitting water with cobalt, Angew. Chem., Int. Ed., 50 (2011)7238–7266.

[28] P. D. Tran, L. Xi, S. K. Batabyal, L. H. Wong, J. Barber, J. S. Chye Loo, Enhancing the photocatalytic efficiency of $TiO_2$ nanopowders for $H_2$ production by using non-noble transition metal co-catalysts, Phys. Chem. Chem. Phys., 14 (2012)11596–11599.

[29] A. Shawky, M. Alhaddad, R.M.M. Mohamed, N.S. Awwad, H.A. Ibrahium, Magnetically separable and visible light-active Ag/$NiCo_2O_4$ nanorods prepared by a simple route for superior photodegradation of atrazine in water, Prog. Nat. Sci. Mater. Int. 30 (2020) 160–167.

[30] H. Yu, J. Yu, B. Cheng, S. Liu Novel preparation and photocatalytic activity of one-dimensional $TiO_2$ hollow structures, Nanotechnology 18 (2007) 065604.

[31] J. Tian, P. Hao, N. Wei, H. Cui, H. Liu, 3D $Bi_2MoO_6$ nanosheet/$TiO_2$ nanobelt heterostructure: enhanced photocatalytic activities and photoelectochemistry performance, ACS Catal. 5 (2015) 4530–4536.

[32] W. Cao, B. Wei, X. Fu, N. Ma, H. Gao, L. Xu, Colored $TiO_2$ hollow spheres for efficient watersplitting photocatalysts, RSC Adv. 6 (2016) 108969.

[33] Q. Jiang, L. Li, J. Bi, S. Liang, M. Liu, Design and Synthesis of $TiO_2$ Hollow Spheres with Spatially Separated Dual Cocatalysts for Efficient Photocatalytic Hydrogen Production, Nanomaterials 7 (2017) 24

[34] M. Xiao, H. Chen, T. Ming, L. Shao, J. Wang, Plasmon-modulated light scattering from gold nanocrystal-decorated hollow mesoporous silica microspheres, ACS Nano 4 (2010) 6565–6572.

[35] M. Retsch, M. Schmelzeisen, H. Butt, E. Thomas, Visible Mie scattering in nonabsorbing hollow sphere powders, Nano Lett. 11 (2011) 1389–1394.

[36] L. Fielding, O. Mykhaylyk, A. Schmid, D. Pontoni, S. Armes, P. Fowler, Visible Mie scattering from hollow silica particles with particulate shells, Chem. Mater. 26 (2014) 1270–1277.

[37] S. Kim, V. Hwang, S. Lee, J. Ha, V. Manoharan, G. Yi, Solution-processable photonic inks of Mie-resonant hollow carbon-silica nanospheres, Small. 15 (2019) 1900931.

[38] X. Yao, Y. Bai, Y. Lee, Z. Qi, X. Liu, Y. Yin, Multi-colored hollow carbon-containing titania nanoshells for anti-counterfeiting applications, J. Mater. Chem. C Mater. Opt. Electron. Devices 7 (2019) 14080–14087.

[39] Y. Li, J. Wang, X. Liu, C. Shen, K. Xie, B. Wei, Au/TiO2 hollow spheres with synergistic effect of plasmonic enhancement and light scattering for improved dyesensitized solar cells, ACS Appl. Mater. Interfaces 9 (2017) 31691–31698.

[40] F. Xie, Y. Li, J. Dou, J. Wu, M. Wei, Facile Synthesis of $SnO_2$ coated urchin-like $TiO_2$ hollow microspheres as efficient scattering layer for dye-sensitized solar cells, J.Power Sources 336 (2016) 143–149

[41] A. A. Ismail, D. W. Bahnemann, L. Robben, V. Yarovyi, M. Wark, Palladium doped porous titania photocatalysts: Impact of mesoporous order and crystallinity, Chemistry of Materials, 22 (2010) 108-116.

[42] G. Dong, H. Hu, X. Huang, Y. Zhang, Y. Bi, Rapid activation of Co3O4 cocatalysts with oxygen vacancies on TiO2 photoanodes for efficient water splitting, J. Mater. Chem. A. 6 (2018) 21003–21009. https://doi.org/10.1039/c8ta08342h.

[43] S. Bala, I. Mondal, A. Goswami, U. Pal, R. Mondal, Co-MOF as a sacrificial template: Manifesting a new Co3O4/TiO2 system with a p-n heterojunction for photocatalytic hydrogen evolution, J. Mater. Chem. A. 3 (2015) 20288–20296. https://doi.org/10.1039/c5ta05210f.

[44] Q. Zhang, Z. Hai, A. Jian, H. Xu, C. Xue, S. Sang, Synthesis of p-Co3O4/n-TiO2 nanoparticles for overall water splitting under visible light irradiation, Nanomaterials. 6 (2016). https://doi.org/10.3390/nano6080138.

[45] X.R. Zhao, Y.Q. Cao, J. Chen, L. Zhu, X. Qian, A.D. Li, D. Wu, Photocatalytic Properties of Co3O4-Coated TiO2 Powders Prepared by Plasma-Enhanced Atomic Layer Deposition, Nanoscale Res. Lett. 12 (2017). https://doi.org/10.1186/s11671-017-2269-4.

[46] Z. Shi, L. Lan, Y. Li, Y. Yang, Q. Zhang, J. Wu, G. Zhang, X. Zhao, Co3O4/TiO2 Nanocomposite Formation Leads to Improvement in Ultraviolet-Visible-Infrared-Driven Thermocatalytic Activity Due to Photoactivation and Photocatalysis-Thermocatalysis Synergetic Effect, ACS Sustain. Chem. Eng. 6 (2018) 16503–16514. https://doi.org/10.1021/acssuschemeng.8b03602.

[47] Z. Lou, Y. Wang, Y. Yang, Y. Wang, C. Qin, R. Liang, X. Chen, Z. Ye, L. Zhu, Carbon sphere template derived hollow nanostructure for photocatalysis and gas sensing, Nanomaterials. 10 (2020). https://doi.org/10.3390/nano10020378.

[48] B. Yu, F. Meng, M.W. Khan, R. Qin, X. Liu, Synthesis of hollow TiO2@g-C3N4/Co3O4 core-shell microspheres for effective photooxidation degradation of tetracycline and MO, Ceram. Int. 46 (2020) 13133–13143. https://doi.org/10.1016/j.ceramint.2020.02.087.

[49] G.M. Tomboc, B.T. Gadisa, J. Joo, H. Kim, K. Lee, Hollow Structured Metal Sulfides for Photocatalytic Hydrogen Generation, ChemNanoMat. 6 (2020) 850–869. https://doi.org/10.1002/cnma.202000125.

[50] Q. Jiang, L. Li, J. Bi, S. Liang, M. Liu, Design and synthesis of Tio2 hollow spheres with spatially separated dual cocatalysts for efficient photocatalytic hydrogen production, Nanomaterials. 7 (2017). https://doi.org/10.3390/nano7020024.

[51] P. She, J. Qin, H. Rao, B. Guan, J. Yu, Spatially separated bimetallic cocatalysts on hollow-structured TiO 2 for photocatalytic hydrogen generation , Mater. Chem. Front. 4 (2020) 1671–1678. https://doi.org/10.1039/d0qm00042f.

[52] B. Fang, Y. Xing, A. Bonakdarpour, S. Zhang, D. P. Wilkinson, Hierarchical CuO−$TiO_2$ Hollow Microspheres for Highly Efficient Photodriven Reduction of $CO_2$ to $CH_4$, ACS Sustainable Chem. Eng. 3(2015)2381−2388.

[53] K. Sing, D. Everett, R. Haul, L. Moscou, R.Pierotti, J.Rouquerol, T. Siemieniewska, Reporting physisorption data for gas/solid systems with special reference to the determination of surface area and porosity. Pure Appl. Chem. 57(1985) 603−619.

[54] Q. Guo, M. Zhang, X. Li, X. Li, H. Li, Y. Lu, X. Song, L. Wang, A novel CuO/$TiO_2$ hollow nanofiber film for non-enzymatic glucose sensing,

RSC Adv., 6(2016) 99969–99976.

[55] J. Yu, H. Guo, S. Davis, S. Mann, Fabrication of hollow inorganic microspheres by chemically induced self-transformation. Adv. Funct. Mater. 16(2006) 2035−2041.

[56] E. Topoglidis, C. J. Campbell, A. E. G. Cass and J. R. Durrant, Factors that affect protein adsorption on nanostructured titania films. A novel spectroelectrochemical application to sensing, Langmuir, 17(2001) 7899–7906.

[57] S. Bala, I. Mondal, A. Goswami, U. Pal, R. Mondal, Co-MOF as a sacrificial template: manifesting a new $Co_3O_4/TiO_2$ system with a p–n heterojunction for photocatalytic hydrogen evolution, J. Mater. Chem. A 3 (2015) 20288-20296.

[58] Q. Zhang, Z. Hai, A. Jian, H. Xu, C. Xue, S. Sang, Synthesis of p-Co3O4/n-TiO2 Nanoparticles for OverallWater Splitting under Visible Light Irradiation, Nanomaterials 6 (2016)138.

[59] I.A. Mkhalid, J.L.G., Fierro, R.M. Mohamed, A. A. Alshahri, Photocatalytic visible-light-driven removal of the herbicide imazapyer using nanocomposites based on mesoporous $TiO_2$ modified with Gd2O3. Appl Nanosci (2020). https://doi.org/10.1007/s13204-020-01479-8.

[60] H. Adhikari, M. Ghimire, C. K. Ranaweera, S. Bhoyate, R. K. Gupta, J. Alam, S. R. Mishra, Synthesis and electrochemical performance of hydrothermally synthesized $Co_3O_4$ nanostructured particles in presence of urea, J. Alloys Compds 708 (2017) 628-638.

[61] M. Zhang, R. Z. Sun, Y. J. Li, Q. M. Shi, L. H. Xie, J.S. Chen, X. H. Xu, H. X. Shi, W. R. Zhao, High $H_2$ Evolution from quantum Cu(II) nanodot-doped two-dimensional ultrathin $TiO_2$ nanosheets with dominant exposed {001} facets for reforming glycerol with multiple electron transport pathways. J. Phys. Chem. C 120 (2016)10746−10756.

[62] A. Diallo, A.C. Beye, T.B. Doyle, E. Park, M. Maaza, Green synthesis of $Co_3O_4$ nanoparticles via *Aspalathus linearis*: Physical properties, Green Chem. Lett. Rev. 8 (2015) 30–36.

[63] Z. Shi, L. Lan, Y. Li, Y. Yang, Q. Zhang, J. Wu, G. Zhang, X. Zhao, $Co_3O_4/TiO_2$ Nanocomposite Formation Leads to Improvement in Ultraviolet−Visible-Infrared-Driven Thermocatalytic Activity Due to Photoactivation and Photocatalysis−Thermocatalysis Synergetic Effect, ACS Sustainable Chem. Eng. 6 (2018)16503−16514.

[64] X-R. Zhao, Y-Q. Cao, J. Chen, L. Zhu, X. Qian, A-D. Li, D. Wu, Photocatalytic Properties of $Co_3O_4$-Coated $TiO_2$ Powders Prepared by Plasma-Enhanced Atomic Layer Deposition, Nanoscale Research Letters 12 (2017) 497.

[65] P. A. Mangrulkar, M. M. Joshi, S. N. Tijare, V. Polshettiwar, Nano cobalt oxides for photocatalytic hydrogen production, International J. hydrogen energy 37 (2012) 10462-10466.

[66] W-D. Wei, X-Y. Liu, S-C. Cui, J-G. Liu, Loading of $Co_3O_4$ onto Pt-modified nitrogendoped $TiO_2$ nanocomposites promotes photocatalytic hydrogen production, RSC Adv. 7 (2017) 25650-25656.

[67] G. Dong, H. Hu, X. Huang, Y. Zhanga, Y. Bi, Rapid activation of $Co_3O_4$ cocatalysts with oxygen vacancies on $TiO_2$ photoanodes for efficient water splitting. J. Mater. Chem. A 6 (2018) 21003–21009.